LANGMUIR

pubs.acs.org/Langmuir Article

Persistent Micelle Corona Chemistry Enables Constant Micelle Core Size with Independent Control of Functionality and Polyelectrolyte Response

Taylor Larison and Morgan Stefik*

Cite This: https://doi.org/10.1021/acs.langmuir.1c01384 Read Online

ACCESS | Metrics & More | Article Recommendations | Supporting Information

ABSTRACT: Polymer micelles have found significant uses in areas such as drug/gene delivery, medical imaging, and as templates for nanomaterials. For many of these applications, the micelle performance depends on its size and chemical functionalization. To date, however, these parameters have often been fundamentally coupled since the equilibrium size of a micelle is a function of the chemical composition in addition to other parameters. Here, we demonstrate a novel processing pathway allowing for the chemical modification to the corona of kinetically trapped "persistent" polymer micelles, termed Persistent Micelle Corona Chemistry (PMCC). Judicious planning is crucial to this size-controlled functionalization where each step requires all reagents and polymer blocks to be compatible with (1) the desired chemistry, (2) micelle persistency, and (3) micelle dispersion. A desired functionalization can be implemented with PMCC by pairing the synthetic planning with polymer solubility databases. Specifically, poly(cyclohexyl methacrylate-*b*-(diethoxyphosphoryl)methyl methacrylate) (PCHMA-*b*-PDEPMMA) was prepared to combine a glassy-core block (PCHMA) for kinetic control with a block (PDEPMMA) that is able to be hydrolyzed to yield acid groups. The processing sequence determines the resulting micelle size distribution where the hydrolyzed-then-micellized sequence yields widely varying micelle dimensions due to equilibration. In contrast, the micellized-then-hydrolyzed sequence maintains kinetically trapped micelles throughout the PMCC process. Statistically significant transmission electron microscopy (TEM) measurements demonstrate that PMCC uniquely enables this functionalization with constant average micelle core dimensions. Furthermore, these kinetically trapped micelles also subsequently maintain constant micelle core size when modifying the Coulombic interactions of the micelle corona via pH changes.

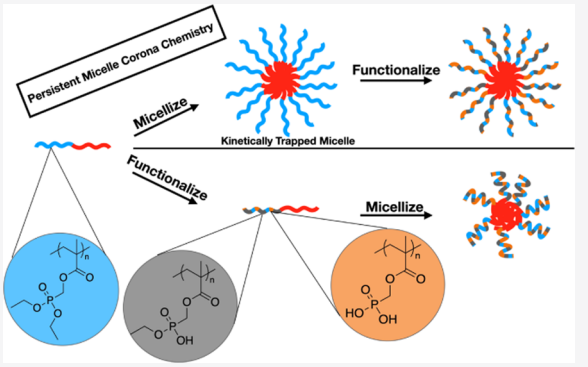

INTRODUCTION

Polyelectrolytes are of broad interest for applications spanning from ion transport,[1−5] to protein binding,[6−10] metal binding,[11−15] wastewater treatment,[16,17] and drug delivery.[18−23] Similarly, block polymer-based micelles have found uses in diverse applications, such as the formation of nanostructured porous materials,[24−31] and for drug delivery.[32−35] For many such applications, the ultimate performance is influenced by the micelle aggregation number (i.e., the core dimension),[36,37] the extent of functionalization,[38−41] or the response of functional groups toward the environment.[20,23,40−42]

The equilibrium aggregation number for a block copolymer micelle is a balance between interfacial enthalpic contributions (χ) and entropic chain stretching contributions, along with other factors including, but not limited to, electrostatic interactions.[43,44] It naturally follows that both the chemical composition and any functional group responses to the environment can alter the equilibrium aggregation number. It is well known that solvent changes can induce micelles to undergo dynamic chain exchange processes that alter the aggregation number and/or the micelle morphology to minimize the free energy of the system.[45] For example, single-chain exchange is a well-documented mechanism.[46−56] Such chain exchange processes can also be kinetically trapped, typically using high-χN conditions. Here, χ is the effective interaction parameter between the core block and the solvent and N scales with the degree of polymerization[a]. With these considerations, a large thermodynamic activation energy for single-chain exchange can impose kinetic control. Another way to restrict chain exchange is with restricted chain mobility via a glassy-core block.[48,52,57] The latter approach is used in the present study to achieve kinetic control of micelles during chemical modifications.

Received: May 24, 2021
Revised: July 14, 2021

We propose a new concept of persistent micelle corona chemistry (PMCC). This concept enables, for the first time to the authors' knowledge, chemical modification to the corona of previously formed and persistent block copolymer micelles. Here, persistence is defined as kinetic entrapment of a constant aggregation number which often corresponds to a constant micelle core dimension. The PMCC approach allows for the independent adjustment of functional group density as well as their responses to the environment while preserving a constant micelle core dimension. In contrast, the typical approach of preparing a series of different chemical modifications followed by micellization can lead to a wide variation of the resulting micelle core dimensions, in part due to the widely varying equilibrium conditions. Block polymer functionalization is accomplished via the use of a monomer with a pendant phosphonated ester that can be hydrolyzed to yield one or two phosphonic acid groups. This functional group is also responsive to pH changes. The pK_a values of phosphonic acid are reported to be 2.75 and 8.2.[58] Decreasing the pH below 2.75 favors protonation of the group, making it charge neutral, whereas increasing the pH above 8.2 favors deprotonation of the group, resulting in an anionic charge. Thus, phosphonic acid groups have a Coulombic response to pH changes. For micelle core immobilization, please note that there are a range of modalities, e.g., high-χN conditions,[28,48,60,61] glassy-core micelles,[52,57] crystalline core micelles,[62−65] and cross-linked core micelles,[66,67] which are compatible with the PMCC concept; however, prior works did not emphasize granular functionalization after micellization. Similarly, polymer brush-grafted nanoparticles enable similar corona tuning typically with a solid inorganic core.[68−70] Here, we opted for a purely block polymer-based strategy for the convenience and modularity of organic chemistry coupled with the future ability to load micelles, e.g., organic drug molecules. It is shown that PMCC enables the preservation of constant micelle core size during both functionalization and subsequent tailoring of the Coulombic interaction strength.

EXPERIMENTAL PROCEDURES

Materials. All materials were used as received unless specified otherwise. Methanol (99.8%, Fisher), diethyl (hydroxymethyl)-phosphonate (≥97.0%, TCI), methacrylic acid (>99%, Alfa Aesar), *N*′*N*-dicyclohexylcarbodiimide (DCC, ≥99%, BeanTown Chemical), 4-cyano-4-(phenylcarbonothioylthio)pentanoic acid (4CPDB, 97% Strem Chemicals), sodium hydroxide (≥97%, Sigma), chloroform (≥99.8%, VWR), tetrahydrofuran (Fisher), methylene chloride (Fisher), acetonitrile (≥99.9%, Sigma), and 4-dimethylaminopyridine (DMAP, >99%, TCI) were used as received. Cyclohexyl methacrylate (≥98.0%, TCI) monomer was run over a basic alumina column prior to use. 2,2′-Azobis(2-methylpropionitrile) (AIBN, Sigma) was recrystallized from methanol. Bromotrimethylsilane (TMSBr, 97%, Chem Impex Intl Inc MS) was stored in the glovebox.

(Diethoxyphosphoryl)methyl methacrylate (DEPMMA) Monomer Synthesis. Diethyl(hydroxymethyl)phosphonate (5 g, 4.27 mL, 29.73 mmol), methacrylic acid (2.56 g, 29.73 mmol), and 15 mL of chloroform were mixed in a round bottom flask. The solution was cooled to 0 °C and sparged with nitrogen for 30 min. A solution of *N*′*N*-dicyclohexylcarbodiimide (DCC) (6.75 g, 32.70 mmol), 4-dimethylaminopyridine (DMAP) (0.40 g, 3.27 mmol), and 5 mL of chloroform was then added in a dropwise manner. The suspension was left to vigorously stir at room temperature for 2 h. The suspension was then filtered and the chloroform was removed using reduced pressure. The crude product was then purified via vacuum distillation at 175 °C. The final product (diethoxyphosphoryl)methyl methacrylate (DEPEMA) was verified using ^{1}H NMR and ^{31}P NMR (Figures S1 and S2).

Poly(cyclohexyl methacrylate) (PCHMA) Synthesis. Cyclohexyl methacrylate (CHMA) (7.50 mL, 42.95 mmol), 2,2′-azobis(2-methylpropionitrile) (AIBN) (8.80 mg, 0.054 mmol), 4-cyano-4-(phenylcarbonothioylthio)pentanoic acid (4CPDB) (100 mg, 0.36 mmol), and 4.50 mL of tetrahydrofuran (THF) were combined in a Schlenk flask and were subjected to three cycles of freeze−pump−thaw. The reaction flask was then brought into an argon-filled glovebox to backfill the flask with argon. The polymerization was then carried out in a preheated oil bath at 70 °C for 16.75 h. Once the polymerization was complete, the reaction was cooled in a freezer before venting and dilution with THF to fully dissolve the viscous product. PCHMA was then precipitated using cold methanol, filtered, and then dried in a vacuum oven overnight. The molar mass of PCHMA was calculated based on the ratio of reversible addition-fragmentation chain-transfer (RAFT) agent to cyclohexyl methacrylate assuming 100% conversion. The molar mass and conversion were quantified using ^{1}H NMR in $CDCl_3$ (Figure S3). The molar-mass dispersity ($Đ$) was verified by gel permeation chromatography (GPC).

PCHMA-*b*-PDEPMMA Diblock Polymer Synthesis. PCHMA-4CPDB (20 k) macroinitiator (3.50 g, 0.17 mmol), 2,2′-azobis(2-methylpropionitrile) (AIBN) (8.54 mg, 0.052 mmol), DEPMMA (6.14 g, 6.54 mL, 26.01 mmol), and 6.85 mL of THF were mixed in a Schlenk flask and were subjected to three cycles of freeze−pump−thaw. The reaction flask was then brought into an argon-filled glovebox to backfill the flask with argon. The polymerization was then carried out in a preheated oil bath at 70 °C for 18.25 h. The reaction was then cooled in a freezer before venting and dilution with THF to fully dissolve the viscous product. PCHMA-*b*-PDEPMMA was then precipitated out using cold hexane, filtered, and then dried in a vacuum oven overnight. The molar mass and conversion were quantified using ^{1}H NMR in $CDCl_3$ (Figure S4). The molar-mass dispersity ($Đ$) was verified by GPC (Table S1).

Glassy-Core Micelle Stock Preparation. PCHMA-*b*-PDEPMMA (52 k) (1 g, 0.2 mmol) was dissolved in 100 mL of methylene chloride. Then, 240 mL of acetonitrile was added dropwise to the stirring solution to induce micelle formation as checked by dynamic light scattering (DLS) (Figure S5). Methylene chloride and excess acetonitrile were removed by rotary evaporation until the concentration of the solution was 10 mg/mL. This micelle stock solution was subjected to three cycles of freeze−pump−thaw and was stored in an argon-filled glovebox.

Micellized-then-Hydrolyzed Method (MH). What follows is a generalized deprotection procedure. In a glovebox, 5 mL of the micelle stock solution was placed in a vial with a stir bar. An equivalent amount of bromotrimethylsilane (TMSBr) dependent on the desired extent of hydrolysis was added to the vial before it was sealed. TMSBr was labeled as 97% purity; however, repeated hydrolysis reactions consistently resulted in 95% conversion: thus, 95% TMSBr purity was assumed for all stoichiometric calculations. The solution was stirred in a preheated oil bath at 50 °C overnight. The suspension was then dried and redispersed in 5 mL of methanol and allowed to stir for 2 h. A small aliquot of the solution was dried and mixed in a solution of 60/40 MeOD/$CDCl_3$ with a drop of deuterium chloride added to protonate all phosphonic acid groups present to verify the extent of deprotection with ^{31}P NMR. A model assuming random hydrolysis was compared to this data. The goodness-of-fit for the model, R^2, was calculated as the sum squared of regression divided by the sum square of the total.

Micelle Solvent Exchange. Micelles that were previously functionalized via deprotection were transferred from methanol to a different solvent. Aqueous sodium hydroxide (1 mM, 3 mL) was added dropwise to 2 mL of 10 mg/mL functionalized micelle stock solution. Subsequently, the methanol was removed by rotary evaporation.

Hydrolyzed-then-Micellized Method (HM). A functionalized micelle stock was dried and redispersed as unimers in 2 mL of THF (relatively nonselective) to remove the effects of the prior processing

https://doi.org/10.1021/acs.langmuir.1c01384
Langmuir XXXX, XXX, XXX−XXX

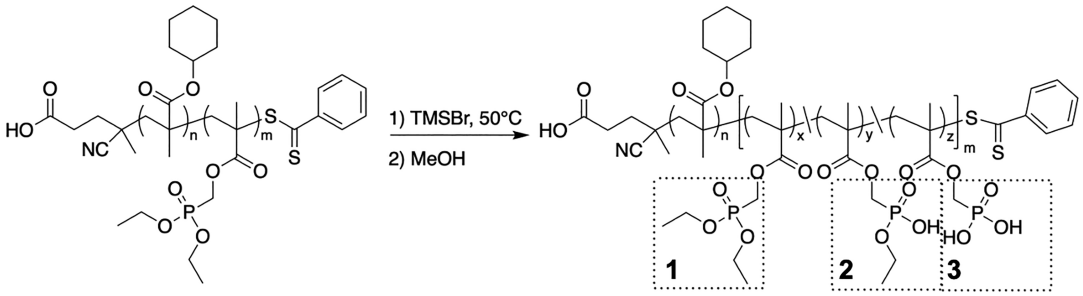

Figure 1. Scheme showing the hydrolysis of PCHMA-*b*-PDEPMMA in acetonitrile using TMSBr followed by solvolysis in methanol. The resulting modified PDEPMMA block contains a random distribution of di-ester(1), mono-acid(2), and di-acid(3) phosphorous functional groups depending on the extent of reaction.

history. Then, an aqueous sodium hydroxide solution (1 mM, 3 mL) was added dropwise to the stirring micelle solution to form micelles. The THF was subsequently removed by rotary evaporation.

DLS Measurements. Aliquots of 2 mL were filtered through 0.2 mm syringe filters into quartz cuvettes and were tightly sealed. Measurements were performed using a Zetasizer Nanoseries ZEN3690 instrument. Measurements were run at 25 °C with 5 min thermal equilibration time prior to each 5 min acquisition. The data for micelle size were analyzed using the refractive index of pure MeOH or pure acetonitrile since the solutions were ∼99% pure solvent. Data were fit with a log-normal distribution corresponding to the mean and standard deviation.

ζ Potential Measurements. Micelles previously dispersed in an aqueous sodium hydroxide solution (1 mM) were dried via evaporation. A solution of 80:20 volume percent THF:methanol was used to dissolve the dried micelle powders and disperse the diblock polymers as unimers with a concentration of 4 mg/mL. Aliquots of 1.2 mL were placed into a quartz cuvette with a dip cell. Measurements were performed using a Zetasizer Nanoseries ZEN3690 instrument. Measurements were run at 25 °C with 5 min thermal equilibration time prior to each acquisition.

Transmission Electron Microscopy (TEM) Measurements. TEM images were acquired using a JEOL 1400 Plus TEM operated in bright field mode with an accelerating voltage of 120 keV. Samples were prepared by placing a single drop of 10 mg/mL micelle solution onto a carbon-coated 300 mesh copper grid purchased from Electron Microscopy Sciences. The solvent was wicked away after 2 min with a filter paper. Samples were then stained by placing one drop of 1% uranyl acetate solution onto each grid for 3 min before wicking the solvent away with filter paper. About 60 measurements were taken from each sample condition to yield statistically relevant metrics for the average, the standard deviation (statistical spread), and the standard-error-of-the-mean (uncertainty of the mean value itself).

RESULTS AND DISCUSSION

The independent control of micelle size (aggregation number), functional group content, and the response to stimuli are of interest for a range of polyelectrolyte applications. Prior examples to date however have struggled to demonstrate independent control of these parameters due often to a reliance upon equilibrium-based processing. Micelles with active chain exchange mechanisms are able to change their aggregation number in response to either this functionalization or any change in the external stimuli. Furthermore, the formation of kinetically trapped micelles after functionalization also leads to different sizes depending on the extent of functionalization, vide infra. Here, we report a pathway called PMCC that sidesteps these challenges by first establishing a specific aggregation number and subsequently preserving this persistency throughout the entire processing pathway. Using this method, chemical functionalization and/or the external stimuli may occur independently while preserving the specific aggregation number. Here, we use glassy-persistent micelles for the sake of arresting chain exchange via core immobility. Even so, judicious planning is crucial since (i) functionalization reactions often have a limited scope of compatible solvents, (ii) functionalization reagents can induce dynamic chain exchange between micelles, and (iii) the corona block solubility can change significantly during functionalization. Below we outline the design criteria for PMCC in terms of (1) polymer design, (2) polymer functionalization, and (3) processing pathway dependence, highlighting the importance of sequence upon maintaining micelle control.

1. Polymer Design. A custom corona block was prepared to enable functionalization as well as a Coulombic stimuli response. Specifically (diethoxyphosphoryl)methyl methacrylate (DEPMMA) was chosen due to the well-studied characteristics of this class of polymers[58,71−76] and the ease of hydrolysis postpolymerization for the phosphonated esters to become acid groups via the McKenna reaction.[58,77] These phosphonic acid moieties have pK_a values of 2.75 and 8.2,[58] allowing for the tailoring of Coulombic interactions in response to pH changes.[43] For the present example, a methacrylate corona block was preferred for facile RAFT polymerization.[78] The DEPMMA monomer synthesis used a Steglich esterification similar to a prior report.[74] The ^{1}H NMR confirmed the successful synthesis of DEPMMA (Figure S1). The DEPMMA monomer can be purified via distillation; however, this step is optional since only benign contaminants remain that are removed during polymer purification. The solubility of the corona block is also crucial to consider. Here, PDEPMMA is soluble in alcohols, THF, chloroform, methylene chloride, and acetonitrile for example, whereas after hydrolysis, the resulting poly(((methacryloyloxy)methyl)-phosphonic acid) is soluble in THF, acetonitrile, water, and alcohols but not chloroform nor methylene chloride. This solubility requirement is important such that the micelles remain dispersed throughout the functionalization process. This particular requirement narrows the list of candidate solvents down to water, alcohols, THF, or acetonitrile. The solvent selection is further constrained by compatibility with the desired reaction(s). Here, the hydrolysis of PDEPMMA is planned via the McKenna reaction, which is incompatible with protic solvents, thus leaving THF and acetonitrile on the list of candidate solvents.

A core block was also carefully selected to demonstrate the PMCC concept. Here, the main role of the core block was to maintain kinetic control of the micelle size and aggregation number. A glassy block was selected for molecular immobilization so long as plasticizing solvents are avoided. At this point,

https://doi.org/10.1021/acs.langmuir.1c01384
Langmuir XXXX, XXX, XXX−XXX

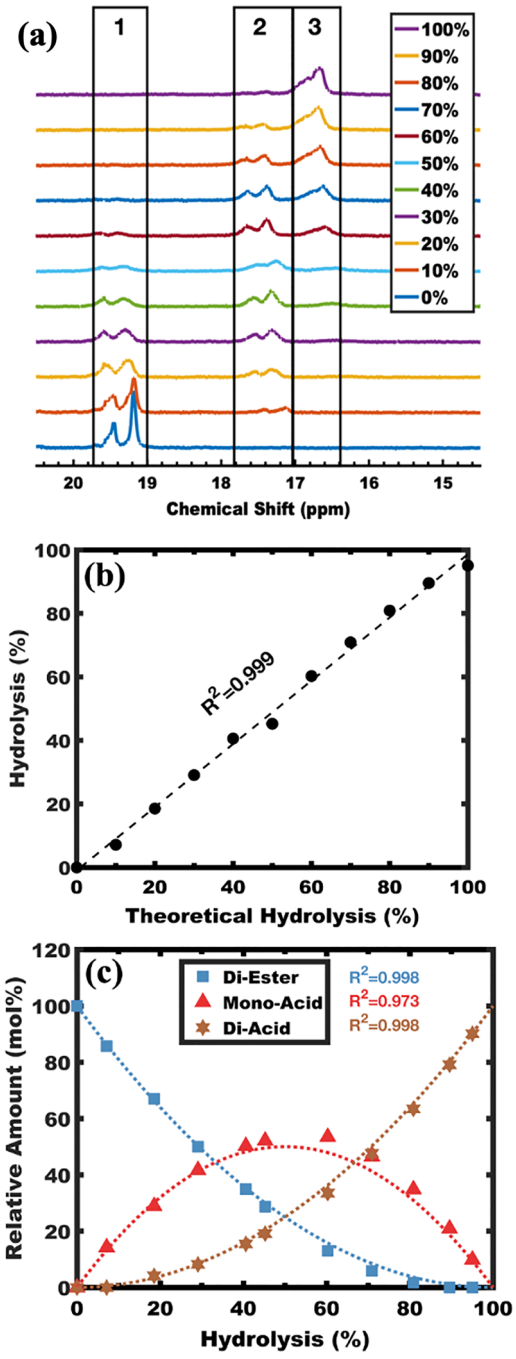

Figure 2. (a) Hydrolysis of the PDEPMMA di-ester (1) to the mono-acid (2) and di-acid (3) products (see Figure 1) were quantified using ^{31}P NMR. (b) Hydrolysis reaction was efficient with high yield (TMSBr 95% purity, R^2 is the Pearson correlation coefficient). (c) Corresponding distributions of phosphorous functional groups (1/2/3) are shown. The dashed lines were calculated based upon equal reactivity (random probability) of di-ester and mono-acid. The R^2 values in panel (c) correspond to the goodness-of-fit. These data correspond to the hydrolysis of preformed PCHMA-*b*-PDEPMMA micelles with glassy cores.

the list of candidate solvents include THF and acetonitrile. Though limiting, the use of known solubility databases[81] and creative polymer chemistry can often yield suitable combinations. For example, our early attempts with poly(methyl methacrylate) (PMMA) and polystyrene (PS) core blocks both failed due to plasticization by THF and acetonitrile. Using databases,[81,82] a search for methacrylates that were more hydrophobic than PS and PMMA to avoid plasticization by acetonitrile while having a T_g above all reaction conditions yielded cyclohexyl methacrylate (CHMA). Please note that this sequence of considerations is not exhaustive but is rather intended to be illustrative of the confluence of factors. Finally, PCHMA is also compatible with our chosen RAFT polymerization method. The CHMA polymerization was allowed to progress until >99% conversion as validated by ^{1}H NMR (Figure S3). The PCHMA was measured using GPC and was found to have a molar-mass dispersity index of 1.08. Subsequently, the PCHMA-4CPDB macroinitiator was used for DEPMMA polymerization to yield PCHMA-*b*-PDEPMMA. The polymerization was allowed to progress to 88% conversion as tracked by ^{1}H NMR (Figure S4). The reaction time was selected to balance polymerization time and conversion yield without any apparent side reactions or other limitations. The final polymer had a molar mass of 52 kg/mol, a composition of 61 wt % PDEPMMA, and a molar-mass dispersity index of 1.12 (Table S1). The core block molecular weight can affect both the micelle size[79] and its glass transition temperature (T_g).[80] Please note that the final PCHMA-*b*-PDEPMMA is amphiphilic and readily form micelles with selective solvents (Figure S5). Thus, a custom block copolymer was prepared for subsequent investigation of the hydrolysis and micellization sequence.

2. Functionalization via Hydrolysis of Pendant Phosphonate groups. The hydrolysis of PDEPMMA was next investigated with the aim of granular functionalization to enable tailoring of the acid content and the associated Coulombic interactions. Here, the McKenna reaction was selected for hydrolysis where TMSBr was added to a micelle solution in acetonitrile to transform the alkyl ester into the corresponding trimethylsilyl ester. Subsequently, methanol was added to induce solvolysis of trimethylsilyl ester, forming the desired phosphonic acid group (Figure 1). A range of TMSBr/phosphonate ratios were examined and the extent of hydrolysis was measured using ^{31}P NMR (Figure 2a). The degree of hydrolysis was found to be quantitative, where the amount of TMSBr directly corresponded to the extent of ester hydrolysis ranging from 0 to 95.05 mol % (Table S2) with a Pearson correlation coefficient of 0.999 (Figure 2b). Each repeat unit of PDEPMMA has a single pendant phosphonate group with two esters that are each available for hydrolysis. Thus, the possible hydrolysis products include both a mono-acid and a di-acid (Figure 1). These specific hydrolysis products were quantified using ^{31}P NMR, where there was a clear separation between di-ester, mono-acid, and di-acid groups (Figure 2a). The peaks at 19.5, 17.5, and 16.5 ppm correspond to the di-ester phosphonate (Figure 2a-1), the mono-acid phosphonate (Figure 2a-2), and the di-acid phosphonate (Figure 2a-3), respectively. The trends of hydrolysis product distribution as a function of TMSBr content are shown in Figure 2c. For example, there was a steady increase in mono-acid content until reaching 60% total hydrolysis at which point the mono-acid content steadily decreased due to its conversion to the di-acid. The measured functional group compositions well matched the theoretical expectations for random and unbiased hydrolysis with goodness-of-fit values exceeding 0.97 (Figure 2c dashed lines). To further validate corona functionalization, measurements of the ζ potential were run on samples containing 0, 40, 60, and 100% degree of hydrolysis (Table S3). The results showed that an increase in the degree of

https://doi.org/10.1021/acs.langmuir.1c01384
Langmuir XXXX, XXX, XXX−XXX

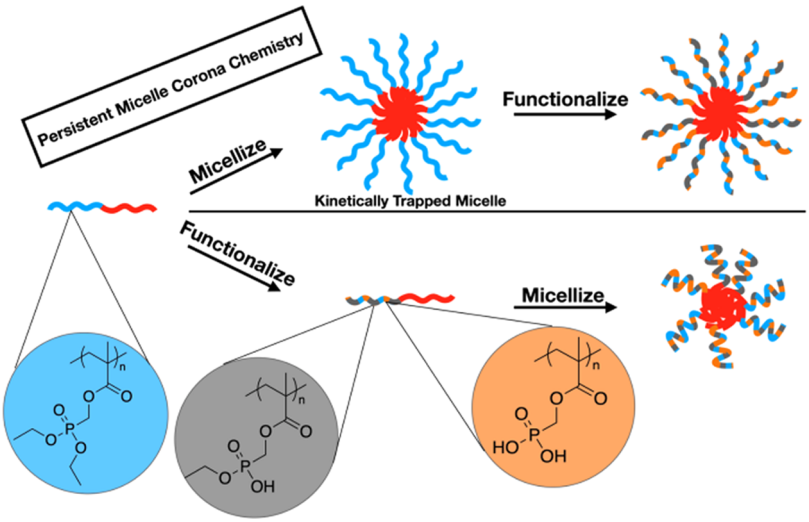

Figure 3. Scheme showing the core size dependence on the synthetic pathway used to functionalize micelles. The top path begins with kinetically trapped polymer micelles and ends with functionalization via hydrolysis ("micellized-then-hydrolyzed"). The bottom path begins with functionalization and ends with micellization ("hydrolyzed-then-micellized"). Only the top path imposes a constant aggregation number throughout the process and was termed Persistent Micelle Corona Chemistry (PMCC).

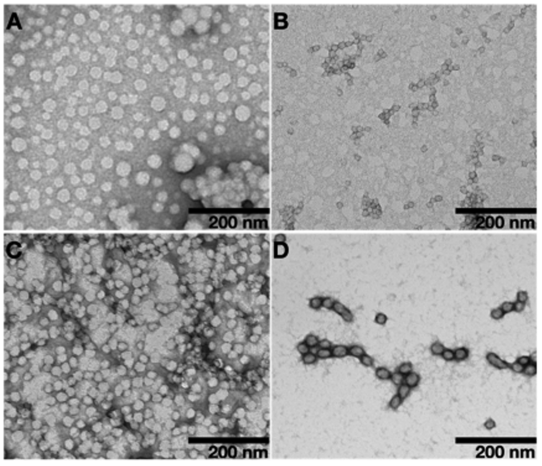

Figure 4. TEM images showing PCHMA-*b*-PDEPMMA micelles dispersed in 1 mM NaOH as a function of the synthesis pathway. The samples were either hydrolyzed-then-micellized (HM, top) or micellized-then-hydrolyzed (MH, bottom). The extent of the hydrolysis reaction varied from 0 to 100%. Data are shown for HM(base)-0 (A), HM(base)-100 (B), MH(base)-0 (C), and MH(base)-100 (D). The samples were stained with uranyl acetate, which selectively associates with the phosphonate coronas (dark) and does not associate with the PCHMA cores (light).

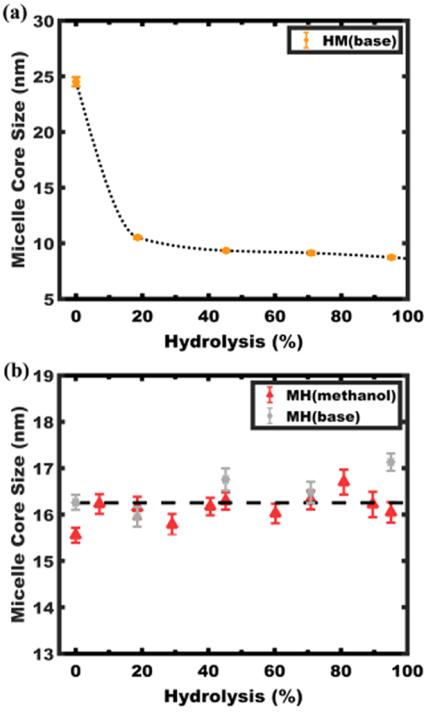

Figure 5. (a) The trend in micelle core size for the hydrolyze-then-micellize sample series dispersed in 1 mM NaOH (HM(base) series) is shown as a function of the degree of hydrolysis. (b) The trends in micelle core size for the micellize-then-hydrolyze sample series dispersed in either methanol (MH(methanol) series) or in 1 mM NaOH (MH(base) series) are shown as a function of the extent of hydrolysis. The error bars correspond to the standard-error-of-the-mean. Please note that the HM-0(base) and MH-0(base) have different average micelle core sizes due to the different processing pathways used for the HM and MH series, respectively.

hydrolysis resulted in a decreasing ζ potential. This trend in ζ potential is consistent with an increase in anionic charge via the formation of phosphonic acid groups. Thus, a block polymer with a tailored and granular functionalization of pendant phosphonate groups was demonstrated.

3. Micelle Formation Pathway Dependence. A specific order of operations is essential to the PMCC concept. The equilibrium size and morphology of diblock polymer micelles is affected in part by Coulombic interactions.[43,44] This dependence is shown first before presenting an example of the PMCC approach. Micelles were prepared from the above series of block polymers with varied extent of functionalization. These block polymers were dispersed as unimers in THF and were then micellized using a basic solution (1 mM NaOH) to favor deprotonation of the phosphonic acid moieties of the PDEPMMA. The THF was subsequently removed selectively by evaporation. This processing sequence was denoted as "hydrolyzed-then-micellized" (HM(base)) (Figure 3 bottom). Here, samples were named for the preparation method and the

https://doi.org/10.1021/acs.langmuir.1c01384
Langmuir XXXX, XXX, XXX−XXX

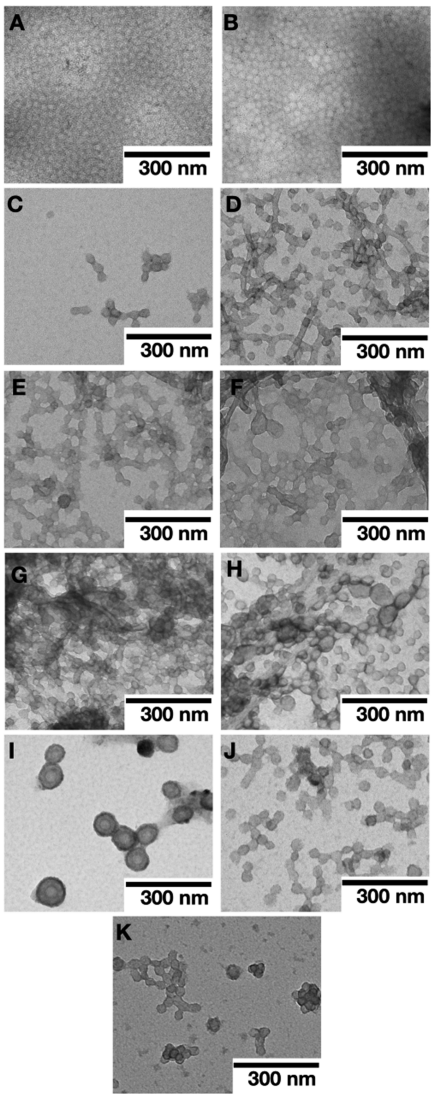

Figure 6. TEM images are shown for PCHMA-*b*-PDEPMMA micelles that were micellized-then-hydrolyzed (MH series). Data are shown for MH(methanol)-0 (A), MH(methanol)-10 (B), MH-(methanol)-20 (C), MH(methanol)-30 (D), MH(methanol)-40 (E), MH(methanol)-50 (F), MH(methanol)-60 (G), MH-(methanol)-70 (H), MH(methanol)-80 (I), MH(methanol)-90 (J), and MH(methanol)-100 (K). Samples were stained with uranyl acetate to darken the PDEPMMA corona.

targeted extent of hydrolysis where HM(base)-100 has 95.1 mol % of ester groups hydrolyzed. The effects of the phosphonic acid content upon the micelle core size were examined using TEM (Figure 4A,B). Here, the core size is a proxy for the aggregation number. An advantage of this TEM data is that it directly quantifies the micelle core size alone in a model-independent fashion. The average micelle core diameters were calculated as the average of 60 measurements for each degree of hydrolysis (Table S4). The TEM samples were prepared by staining with 1% uranyl acetate that selectively associated with the PDEPMMA coronas (dark) and did not stain the PCHMA core (light). This series of HM(base) samples had a monotonically decreasing average core diameter as the extent of hydrolysis increased (Figure 5a). For example, HM(base)-0 and HM(base)-100 had average core diameters of 24.51 and 8.73 nm, respectively, a significant 3× variation in core diameter suggesting a 27× variation in aggregation number based upon the change in volume (Table S4 and Figure 5a). This trend is consistent with increasing repulsive electrostatic interactions favoring micelles with a lower aggregation number to increase the distance between corona blocks.[44] Thus, the hydrolyzed-then-micellized route leads to drastic changes in the aggregation number and size of the micelle cores.

The inhibition of chain exchange mechanisms while functionalizing is the essence of the PMCC concept (Figure 3 top). Toward this end, the PCHMA-*b*-PDEPMMA was dissolved as unimers in THF and was next micellized by adding acetonitrile as checked by DLS (Figure S5). The DLS data were used to identify micelle formation but were not used to assess the core size since DLS also includes the corona block and solvation shell contributions. Next, the complete removal of good solvent (THF) is necessary to kinetically trap the micelles through immobilization of the glassy PCHMA core block. Please note that one must remove all traces of good solvent to avoid plasticization of the core block. We note that the PMCC concept does not explicitly require the use of a glassy core since high-χN solution conditions can also suppress chain exchange and micelle reorganization.[28,29,48,60,61] These glassy-persistent micelles were subsequently functionalized via hydrolysis. Again, the phosphonated esters of PDEPMMA blocks were subjected to quantitative hydrolysis using TMSBr to result in a range of hydrolysis extents from 0 to 95.1 (mol %) (Table S2). After functionalization, the sample series was dried to a powder, and then redispersed in methanol followed by the dropwise addition of the same 1 mM NaOH base solution and evaporative removal of the methanol. This series was termed as "micellized-then-hydrolyzed," specifically dispersed in basic media (MH(base)). Again, the deprotonation of the phosphonic acid moieties (pH 11) and the associated increase in corona charge density is expected to lead to a large change in the equilibrium aggregation number. The observed trend in aggregation number was again measured using TEM imaging (Figure 4C,D). In contrast to the 3× variation in core diameter size across the HM(base) series, the MH(base) series had core sizes ranging from 16.0 ± 0.2 to 17.1 ± 0.2 nm, consistent with minor random variation about a constant mean (Table S4 and Figure 5b). It can be inferred that these micelles did not progress toward the various equilibrium aggregation numbers due to kinetic entrapment. We note that this approach thus enables a series with a constant core diameter and variable charge density. These data demonstrate the remarkable impact of the synthetic pathway dependence upon the final micelle characteristics. Thus, it was shown that the PMCC method enables micelle series with variable functionalization and constant aggregation number.

Finally, we examine the robustness of these persistent micelles toward a wide-sweeping change in Coulombic interaction strength. The micellized-then-hydrolyzed series were also characterized at the point of redispersion into neat methanol, termed (MH(methanol)). TEM images of this sample series are shown in Figure 6. Again, TEM measurements reveal that the average core sizes were relatively constant, ranging from 15.6 ± 0.2 to 16.7 ± 0.3 nm, again suggestive of minor random variation about a constant mean (Table S5 and Figure 5b). Comparison of sample series MH(base) to MH(methanol) shows that a constant nominal core size is maintained in multiple solvents. Furthermore, these series show constant nominal core size with widely varying

https://doi.org/10.1021/acs.langmuir.1c01384
Langmuir XXXX, XXX, XXX−XXX

charge density since the MH(base) series had a pH of 11 that deprotonates all phosphonic acid moieties. This constant core diameter again demonstrates a lack of chain exchange during the significant changes in Coulombic interaction strength. Thus, the PMCC approach enables micelle series which preserve constant aggregation number during variable functionalization and switchable pH stimuli that modulate the Coulombic interaction strength. This is the first demonstration, to the best of the authors' knowledge, that separates micelle core size control from subsequent changes to the corona chemistry.

4. CONCLUSIONS

This work demonstrates that the PMCC enables constant micelle core size while functionalizing the micelle corona and furthermore while changing the strength of the corona Coulombic interactions. The judicious selection of polymer chemistry, processing solvents, and processing pathway is crucial to maintaining kinetic micelle control while conducting chemical transformations upon the corona chains. In contrast, the typical approach of functionalize-then-micellize was shown to lead to wide variation of the resulting micelle aggregation number. The PMCC concept was demonstrated using the hydrolysis and subsequent deprotonation of PDEPMMA coronas on PCHMA-*b*-PDEPMMA micelles as verified by NMR and TEM experiments. Here, the combination of a glassy PCHMA core block while performing functionalization in a solvent (i) did not plasticize PCHMA core blocks, (ii) solvated PDEPMMA corona chains throughout the entire functionalization process, and (iii) was compatible with the functionalization reaction. Though these constraints are many, the use of solubility databases and creative polymer chemistry often enable the identification of suitable combinations. It was shown that careful constraint management enabled the extent of functionalization and the charge density response toward pH to be fully tunable while maintaining kinetic micelle control. Using this method, one can independently study the effects of varied corona acid content of their choosing without associated changes to the nominal micelle core size. Similarly, one can independently tailor the micelle charge density. It is anticipated that future PMCC examples will enable diverse single-variable micelle studies with diverse chemistries.

■ ASSOCIATED CONTENT

Supporting Information

The Supporting Information is available free of charge at https://pubs.acs.org/doi/10.1021/acs.langmuir.1c01384.

^{1}H NMR spectra for all compounds, DLS plot, and tables for: polymer characteristics, ζ potentials, hydrolysis percentages, and TEM measurements (PDF)

■ AUTHOR INFORMATION

Corresponding Author

Morgan Stefik − *Department of Chemistry and Biochemistry, University of South Carolina, Columbia, South Carolina 29208, United States;* Present Address: Department of Chemistry and Biochemistry, University of South Carolina, Columbia, South Carolina 29208, United States; orcid.org/0000-0002-2645-7442; Email: morgan@stefikgroup.com

Author

Taylor Larison − *Department of Chemistry and Biochemistry, University of South Carolina, Columbia, South Carolina 29208, United States*

Complete contact information is available at: https://pubs.acs.org/10.1021/acs.langmuir.1c01384

Author Contributions

The manuscript was written through the contributions of all authors. All authors have given approval to the final version of the manuscript.

Funding

NSF-OIA-1655740 DMR-1752615

Notes

The authors declare no competing financial interest.

■ ACKNOWLEDGMENTS

T.L. was supported by the National Science Foundation EPSCoR Program under NSF Award #OIA-1655740. M.S. acknowledges support by a National Science Foundation CAREER Award (DMR-1752615). This work made use of the South Carolina SAXS Collaborative.

■ ADDITIONAL NOTE

[a]The conventional definition for N in the context of effective interaction parameters equals the chain/block molecular volume divided by the common segment reference volume of 0.118 nm^3.[59] Thus, this N is directly proportional to both the degree of polymerization and the molecular weight, but it is generally not equal to either.

■ REFERENCES

(1) Farhat, T. R.; Schlenoff, J. B. Ion Transport and Equilibria in Polyelectrolyte Multilayers. *Langmuir* **2001**, *17*, 1184−1192.

(2) Kelly, K. D.; Fares, H. M.; Abou Shaheen, S.; Schlenoff, J. B. Intrinsic Properties of Polyelectrolyte Multilayer Membranes: Erasing the Memory of the Interface. *Langmuir* **2018**, *34*, 3874−3883.

(3) Harris, M. A.; Heres, M. F.; Coote, J.; Wenda, A.; Strehmel, V.; Stein, G. E.; Sangoro, J. Ion Transport and Interfacial Dynamics in Disordered Block Copolymers of Ammonium-Based Polymerized Ionic Liquids. *Macromolecules* **2018**, *51*, 3477−3486.

(4) Paren, B. A.; Thurston, B. A.; Neary, W. J.; Kendrick, A.; Kennemur, J. G.; Stevens, M. J.; Frischknecht, A. L.; Winey, K. I. Percolated Ionic Aggregate Morphologies and Decoupled Ion Transport in Precise Sulfonated Polymers Synthesized by Ring-Opening Metathesis Polymerization. *Macromolecules* **2020**, *53*, 8960−8973.

(5) Krasemann, L.; Tieke, B. Selective Ion Transport across Self-Assembled Alternating Multilayers of Cationic and Anionic Polyelectrolytes. *Langmuir* **2000**, *16*, 287−290.

(6) Xu, X.; Angioletti-Uberti, S.; Lu, Y.; Dzubiella, J.; Ballauff, M. Interaction of Proteins with Polyelectrolytes: Comparison of Theory to Experiment. *Langmuir* **2019**, *35*, 5373−5391.

(7) Guo, S.; Zhu, X.; Li, M.; Shi, L.; Ong, J. L. T.; Jańczewski, D.; Neoh, K. G. Parallel Control over Surface Charge and Wettability Using Polyelectrolyte Architecture: Effect on Protein Adsorption and Cell Adhesion. *ACS Appl. Mater. Interfaces* **2016**, *8*, 30552−30563.

(8) Park, J. M.; Muhoberac, B. B.; Dubin, P. L.; Xia, J. Effects of Protein Charge Heterogeneity in Protein-Polyelectrolyte Complexation. *Macromolecules* **1992**, *25*, 290−295.

(9) Kembaren, R.; Fokkink, R.; Westphal, A. H.; Kamperman, M.; Kleijn, J. M.; Borst, J. W. Balancing Enzyme Encapsulation Efficiency and Stability in Complex Coacervate Core Micelles. *Langmuir* **2020**, *36*, 8494−8502.

(10) Anikin, K.; Röcker, C.; Wittemann, A.; Wiedenmann, J.; Ballauff, M.; Nienhaus, G. U. Polyelectrolyte-Mediated Protein Adsorption: Fluorescent Protein Binding to Individual Polyelectrolyte Nanospheres. *J. Phys. Chem. B* **2005**, *109*, 5418−5420.
(11) Wang, T. C.; Rubner, M. F.; Cohen, R. E. Polyelectrolyte Multilayer Nanoreactors for Preparing Silver Nanoparticle Composites: Controlling Metal Concentration and Nanoparticle Size. *Langmuir* **2002**, *18*, 3370−3375.
(12) Zhu, T.; Sha, Y.; Yan, J.; Pageni, P.; Rahman, M. A.; Yan, Y.; Tang, C. Metallo-Polyelectrolytes as a Class of Ionic Macromolecules for Functional Materials. *Nat. Commun.* **2018**, *9*, No. 4329.
(13) Milsom, E. V.; Novak, J.; Green, S. J.; Zhang, X.; Stott, S. J.; Mortimer, R. J.; Edler, K.; Marken, F. Layer-by-Layer Deposition of Open-Pore Mesoporous TiO 2- Nafion Film Electrodes. *J. Solid State Electrochem.* **2007**, *11*, 1109−1117.
(14) Borkovec, M.; Koper, G. J. M.; Piguet, C. Ion Binding to Polyelectrolytes. *Curr. Opin. Colloid Interface Sci.* **2006**, *11*, 280−289.
(15) Nie, H.; Schauser, N. S.; Self, J. L.; Tabassum, T.; Oh, S.; Geng, Z.; Jones, S. D.; Zayas, M. S.; Reynolds, V. G.; Chabinyc, M. L.; Hawker, C. J.; Han, S.; Bates, C. M.; Segalman, R. A.; Read De Alaniz, J. Light-Switchable and Self-Healable Polymer Electrolytes Based on Dynamic Diarylethene and Metal-Ion Coordination. *J. Am. Chem. Soc.* **2021**, *143*, 1562−1569.
(16) Ge, Q.; Wang, P.; Wan, C.; Chung, T. S. Polyelectrolyte-Promoted Forward Osmosis-Membrane Distillation (FO-MD) Hybrid Process for Dye Wastewater Treatment. *Environ. Sci. Technol.* **2012**, *46*, 6236−6243.
(17) Bolto, B.; Gregory, J. Organic Polyelectrolytes in Water Treatment. *Water Res.* **2007**, *41*, 2301−2324.
(18) Nishiyama, N.; Kataoka, K. Current State, Achievements, and Future Prospects of Polymeric Micelles as Nanocarriers for Drug and Gene Delivery. *Pharmacol. Ther.* **2006**, *112*, 630−648.
(19) Sharma, V.; Sundaramurthy, A. Multilayer Capsules Made of Weak Polyelectrolytes: A Review on the Preparation, Functionalization and Applications in Drug Delivery. *Beilstein J. Nanotechnol.* **2020**, *11*, 508−532.
(20) Han, U.; Seo, Y.; Hong, J. Effect of PH on the Structure and Drug Release Profiles of Layer-by-Layer Assembled Films Containing Polyelectrolyte, Micelles, and Graphene Oxide. *Sci. Rep.* **2016**, *6*, No. 24158.
(21) Hu, S. H.; Tsai, C. H.; Liao, C. F.; Liu, D. M.; Chen, S. Y. Controlled Rupture of Magnetic Polyelectrolyte Microcapsules for Drug Delivery. *Langmuir* **2008**, *24*, 11811−11818.
(22) Lai, W. F.; Shum, H. C. Hypromellose-Graft-Chitosan and Its Polyelectrolyte Complex as Novel Systems for Sustained Drug Delivery. *ACS Appl. Mater. Interfaces* **2015**, *7*, 10501−10510.
(23) Yang, Q.; Wang, S.; Fan, P.; Wang, L.; Di, Y.; Lin, K.; Xiao, F. S. PH-Responsive Carrier System Based on Carboxylic Acid Modified Mesoporous Silica and Polyelectrolyte for Drug Delivery. *Chem. Mater.* **2005**, *17*, 5999−6003.
(24) Templin, M.; Franck, A.; Du Chesne, A.; Leist, H.; Zhang, Y.; Ulrich, R.; Schädler, V.; Wiesner, U. Organically Modified Aluminosilicate Mesostructures from Block Copolymer Phases. *Science* **1997**, *278*, 1795−1798.
(25) Zhao, D.; Feng, J.; Huo, Q.; Melosh, N.; Fredrickson, G. H.; Chmelka, B. F.; Stucky, G. D. Triblock Copolymer Syntheses of Mesoporous Silica with Periodic 50 to 300 Angstrom Pores. *Science* **1998**, *279*, 548−552.
(26) Urade, V. N.; Hillhouse, H. W. Synthesis of Thermally Stable Highly Ordered Nanoporous Tin Oxide Thin Films with a 3D Face-Centered Orthorhombic Nanostructure. *J. Phys. Chem. B* **2005**, *109*, 10538−10541.
(27) Warren, S. C.; Messina, L. C.; Slaughter, L. S.; Kamperman, M.; Zhou, Q.; Gruner, S. M.; DiSalvo, F. J.; Wiesner, U. Ordered Mesoporous Materials from Metal Nanoparticle-Block Copolymer Self-Assembly. *Science* **2008**, *320*, 1748−1752.
(28) Lantz, K. A.; Clamp, N. B.; van den Bergh, W.; Sarkar, A.; Stefik, M. Full Gamut Wall Tunability from Persistent Micelle Templates via Ex Situ Hydrolysis. *Small* **2019**, *15*, No. 1900393.
(29) van den Bergh, W.; Lokupitiya, H. N.; Vest, N. A.; Reid, B.; Guldin, S.; Stefik, M. Nanostructure Dependence of T-Nb2O5 Intercalation Pseudocapacitance Probed Using Tunable Isomorphic Architectures. *Adv. Funct. Mater.* **2021**, *31*, No. 2007826.
(30) Peters, K.; Lokupitiya, H. N.; Sarauli, D.; Labs, M.; Pribil, M.; Rathouský, J.; Kuhn, A.; Leister, D.; Stefik, M.; Fattakhova-Rohlfing, D. Nanostructured Antimony-Doped Tin Oxide Layers with Tunable Pore Architectures as Versatile Transparent Current Collectors for Biophotovoltaics. *Adv. Funct. Mater.* **2016**, *26*, 6682−6692.
(31) Bolton, J.; Bailey, T. S.; Rzayev, J. Large Pore Size Nanoporous Materials from the Self-Assembly of Asymmetric Bottlebrush Block Copolymers. *Nano Lett.* **2011**, 998−1001.
(32) Kataoka, K.; Harada, A.; Nagasaki, Y. Block Copolymer Micelles for Drug Delivery: Design, Characterization and Biological Significance. *Adv. Drug Delivery Rev.* **2012**, *64*, 37−48.
(33) Mura, S.; Nicolas, J.; Couvreur, P. Stimuli-Responsive Nanocarriers for Drug Delivery. *Nat. Mater.* **2013**, *12*, 991−1003.
(34) Chopra, P.; Hao, J.; Li, S. K. Sustained Release Micellar Carrier Systems for Iontophoretic Transport of Dexamethasone across Human Sclera. *J. Controlled Release* **2012**, *160*, 96−104.
(35) Lee, E. S.; Gao, Z.; Kim, D.; Park, K.; Kwon, I. C.; Bae, Y. H. Super PH-Sensitive Multifunctional Polymeric Micelle for Tumor PHe Specific TAT Exposure and Multidrug Resistance. *J. Controlled Release* **2008**, *129*, 228−236.
(36) Anraku, Y.; Kishimura, A.; Kobayashi, A.; Oba, M.; Kataoka, K. Size-Controlled Long-Circulating PICsome as a Ruler to Measure Critical Cut-off Disposition Size into Normal and Tumor Tissues. *Chem. Commun.* **2011**, *47*, 6054−6056.
(37) Nel, A. E.; Mädler, L.; Velegol, D.; Xia, T.; Hoek, E. M. V.; Somasundaran, P.; Klaessig, F.; Castranova, V.; Thompson, M. Understanding Biophysicochemical Interactions at the Nano-Bio Interface. *Nat. Mater.* **2009**, *8*, 543−557.
(38) Sanchez, I. C.; Eby, R. K. Thermodynamics and Crystallization of Random Copolymers. *Macromolecules* **1975**, *8*, 638−641.
(39) Dai, C.-A.; Dair, B. J.; Dai, K. H.; Ober, C. K.; Kramer, E. J.; Hui, C. Y.; Jelinski, L.W. Reinforcement of Polymer Interfaces with Random Copolymers. *Phys. Rev. Lett.* **1994**, *73*, 2472−2475.
(40) Nylander, T.; Samoshina, Y.; Lindman, B. Formation of Polyelectrolyte-Surfactant Complexes on Surfaces. *Adv. Colloid Interface Sci.* **2006**, *123*−*126*, 105−123.
(41) Li, L.; Raghupathi, K.; Song, C.; Prasad, P.; Thayumanavan, S. Self-Assembly of Random Copolymers. *Chem. Commun.* **2014**, *50*, 13417−13432.
(42) Cho, J.; Hong, J.; Char, K.; Caruso, F. Nanoporous Block Copolymer Micelle/Micelle Multilayer Films with Dual Optical Properties. *J. Am. Chem. Soc.* **2006**, *128*, 9935−9942.
(43) Linse, P. *Amphiphilic Block Copolymers Self-Assembly and Applications*; Alexandridis, P.; Lindman, B., Eds.; Elsevier, 2000; pp 13−40.
(44) Lee, A. S.; Bütün, V.; Vamvakaki, M.; Armes, S. P.; Pople, J. A.; Gast, A. P. Structure of PH-Dependent Block Copolymer Micelles: Charge and Ionic Strength Dependence. *Macromolecules* **2002**, *35*, 8540−8551.
(45) Luo, L.; Eisenberg, A. Thermodynamic Size Control of Block Copolymer Vesicles in Solution. *Langmuir* **2001**, *17*, 6804−6811.
(46) Lund, R.; Willner, L.; Richter, D.; Dormidontova, E. E. Equilibrium Chain Exchange Kinetics of Diblock Copolymer Micelles: Tuning and Logarithmic Relaxation. *Macromolecules* **2006**, *39*, 4566−4575.
(47) Jain, S.; Bates, F. S. Consequences of Nonergodicity in Aqueous Binary PEO-PB Micellar Dispersions. *Macromolecules* **2004**, *37*, 1511−1523.
(48) Lu, J.; Bates, F. S.; Lodge, T. P. Chain Exchange in Binary Copolymer Micelles at Equilibrium: Confirmation of the Independent Chain Hypothesis. *ACS Macro Lett.* **2013**, *2*, 451−455.
(49) Lu, J.; Bates, F. S.; Lodge, T. P. Addition of Corona Block Homopolymer Retards Chain Exchange in Solutions of Block Copolymer Micelles. *Macromolecules* **2016**, *49*, 1405−1413.

https://doi.org/10.1021/acs.langmuir.1c01384
Langmuir XXXX, XXX, XXX−XXX

(50) Choi, S. H.; Bates, F. S.; Lodge, T. P. Molecular Exchange in Ordered Diblock Copolymer Micelles. *Macromolecules* **2011**, *44*, 3594−3604.
(51) Lu, J.; Bates, F. S.; Lodge, T. P. Remarkable Effect of Molecular Architecture on Chain Exchange in Triblock Copolymer Micelles. *Macromolecules* **2015**, *48*, 2667−2676.
(52) Lu, J.; Choi, S.; Bates, F. S.; Lodge, T. P. Molecular Exchange in Diblock Copolymer Micelles: Bimodal Distribution in Core-Block Molecular Weights. *ACS Macro Lett.* **2012**, *1*, 982−985.
(53) Dormidontova, E. E. Micellization Kinetics in Block Copolymer Solutions: Scaling Model. *Macromolecules* **1999**, *32*, 7630−7644.
(54) Halperin, A.; Alexander, S. Polymeric Micelles: Their Relaxation Kinetics. *Macromolecules* **1989**, *22*, 2403−2412.
(55) Meli, L.; Santiago, J. M.; Lodge, T. P. Path-Dependent Morphology and Relaxation Kinetics of Highly Amphiphilic Diblock Copolymer Micelles in Ionic Liquids. *Macromolecules* **2010**, *43*, 2018−2027.
(56) Kelley, E. G.; Murphy, R. P.; Seppala, J. E.; Smart, T. P.; Hann, S. D.; Sullivan, M. O.; Epps, T. H. Size Evolution of Highly Amphiphilic Macromolecular Solution Assemblies via a Distince Bimodal Pathway. *Nat. Commun.* **2014**, *5*, No. 3599.
(57) Williams, E. R.; McMahon, P. L.; Reynolds, J. E.; Snider, J. L.; Stavila, V.; Allendorf, M. D.; Stefik, M. Tailored Porous Carbons Enabled by Persistent Micelles with Glassy Cores. *Mater. Adv.* **2021**, DOI: 10.1039/d1ma00146a.
(58) Canniccioni, B.; Monge, S.; David, G.; Robin, J. J. RAFT Polymerization of Dimethyl(Methacryloyloxy)Methyl Phosphonate and Its Phosphonic Acid Derivative: A New Opportunity for Phosphorus-Based Materials. *Polym. Chem.* **2013**, *4*, 3676−3685.
(59) Choi, S.; Bates, F. S.; Lodge, T. P. *Structure of Poly (Styrene- b -Ethylene- Alt -Propylene) Diblock Copolymer Micelles In Squalane* **2009**, *113*, 13840−13848.
(60) Schillen, K.; Yekta, A.; Ni, S.; Winnik, M. A. Characterization by Fluorescence Energy Transfer of the Core of Polyisoprene-Poly(Methyl Methacrylate) Diblock Copolymer Micelles. Strong Segregation in Acetonitrile. *Macromolecules* **1998**, *9297*, 210−212.
(61) Lokupitiya, H. N.; Jones, A.; Reid, B.; Guldin, S.; Stefik, M. Ordered Mesoporous to Macroporous Oxides with Tunable Isomorphic Architectures: Solution Criteria for Persistent Micelle Templates. *Chem. Mater.* **2016**, *28*, 1653−1667.
(62) Massey, J. A.; Temple, K.; Cao, L.; Rharbi, Y.; Raez, J.; Winnik, M. A.; Manners, I. Self-Assembly of Organometallic Block Copolymers: The Role of Crystallinity of the Core-Forming Polyferrocene Block in the Micellar Morphologies Formed by Poly(Ferrocenylsilane-b-Dimethylsiloxane) in n-Alkane Solvents. *J. Am. Chem. Soc.* **2000**, *122*, 11577−11584.
(63) Raez, J.; Manners, I.; Winnik, M. A. Nanotubes from the Self-Assembly of Asymmetric Crystalline-Coil Poly(Ferrocenylsilane-Siloxane) Block Copolymers. *J. Am. Chem. Soc.* **2002**, *124*, 10381−10395.
(64) Gädt, T.; Ieong, N. S.; Cambridge, G.; Winnik, M. A.; Manners, I. Complex and Hierarchical Micelle Architectures from Diblock Copolymers Using Living, Crystallization-Driven Polymerizations. *Nat. Mater.* **2009**, *8*, 144−150.
(65) Guerin, G.; Rupar, P.; Molev, G.; Manners, I.; Jinnai, H.; Winnik, M. A. Lateral Growth of 1D Core-Crystalline Micelles upon Annealing in Solution. *Macromolecules* **2016**, *49*, 7004−7014.
(66) O'Reilly, R. K.; Joralemon, M. J.; Wooley, K. L.; Hawker, C. J. Functionalization of Micelles and Shell Cross-Linked Nanoparticles Using Click Chemistry. *Chem. Mater.* **2005**, *17*, 5976−5988.
(67) O'reilly, R. K.; Hawker, C. J.; Wooley, K. L. Cross-Linked Block Copolymer Micelles: Functional Nanostructures of Great Potential and Versatility. *Chem. Soc. Rev.* **2006**, *35*, 1068−1083.
(68) Li, C.; Benicewicz, B. C. Synthesis of Well-Defined Polymer Brushes Grafted onto Silica Nanoparticles via Surface Reversible Addition-Fragmentation Chain Transfer Polymerization. *Macromolecules* **2005**, *38*, 5929−5936.
(69) Kumar, S. K.; Jouault, N.; Benicewicz, B.; Neely, T. Nanocomposites with Polymer Grafted Nanoparticles. *Macromolecules* **2013**, *46*, 3199−3214.
(70) Zhao, D.; Di Nicola, M.; Khani, M. M.; Jestin, J.; Benicewicz, B. C.; Kumar, S. K. Self-Assembly of Monodisperse versus Bidisperse Polymer-Grafted Nanoparticles. *ACS Macro Lett.* **2016**, *5*, 790−795.
(71) Falireas, P. G.; Negrell, C.; David, G. Synthesis and Aqueous Solution Properties of an Amino Bisphosphonate Methacrylate Homopolymer via RAFT Polymerization. *Polymers* **2018**, *10*, No. 711.
(72) Monge, S.; Canniccioni, B.; David, G.; Robin, J. *Phosphorus-Based Polymers: From Synthesis to Applications*; Monge, S.; David, G., Eds.; Royal Society of Chemistry, 2014; pp 1−18.
(73) Graillot, A.; Monge, S.; Faur, C.; Bouyer, D.; Robin, J. J. Synthesis by RAFT of Innovative Well-Defined (Co)Polymers from a Novel Phosphorus-Based Acrylamide Monomer. *Polym. Chem.* **2013**, *4*, 795−803.
(74) Brondino, C.; Boutevin, B.; Parisi, J. P.; Schrynemackers, J. Adhesive Properties onto Galvanized Steel Plates of Grafted Poly(Vinylidene Fluoride) Powders with Phosphonated Acrylates. *J. Appl. Polym. Sci.* **1999**, *72*, 611−620.
(75) El Asri, Z.; Chougrani, K.; Negrell-Guirao, C.; David, G.; Boutevin, B.; Loubat, C. An Efficient Process for Synthesizing and Hydrolyzing a Phosphonated Methacrylate: Investigation of the Adhesive and Anticorrosive Properties. *J. Polym. Sci., Part A: Polym. Chem.* **2008**, *46*, 4794−4803.
(76) Jang, S.; Kim, S. Y.; Jung, H. Y.; Park, M. J. Phosphonated Polymers with Fine-Tuned Ion Clustering Behavior: Toward Efficient Proton Conductors. *Macromolecules* **2018**, *51*, 1120−1128.
(77) Justyna, K.; Małolepsza, J.; Kusy, D.; Maniukiewicz, W.; Błażewska, K. M. The McKenna Reaction − Avoiding Side Reactions in Phosphonate Deprotection. *Beilstein J. Org. Chem.* **2020**, *16*, 1436−1446.
(78) Keddie, D. J.; Moad, G.; Rizzardo, E.; Thang, S. H. RAFT Agent Design and Synthesis. *Macromolecules* **2012**, *45*, 5321−5342.
(79) Lund, R.; Willner, L.; Richter, D. Kinetics of Block Copolymer Micelles Studied by Small-Angle Scattering Methods. In *Controlled Polymerization and Polymeric Structures*; Abe, A.; Lee, K.-S.; Leibler, L.; Kobayashi, S., Eds.; Springer International Publishing: Cham, 2013; pp 51−158.
(80) Fox, T. G.; Flory, P. J. Second-Order Transition Temperatures and Related Properties of Polystyrene. I. Influence of Molecular Weight. *J. Appl. Phys.* **1950**, *21*, 581−591.
(81) Mark, J. E. *Polymer Data Handbook*; Mark, J. E., Ed.; Oxford University Press, 1999; pp 1−1003.
(82) Poylmer Properties Database. https://polymerdatabase.com/polymer%20physics/Polymer%20Tg.html (accessed Sep 10, 2020).

https://doi.org/10.1021/acs.langmuir.1c01384
Langmuir XXXX, XXX, XXX−XXX